PCCP

RSC Publishing

PAPER

View Article Online
View Journal | View Issue

Understanding CeO_2 as a Deacon catalyst by probe molecule adsorption and *in situ* infrared characterisations†

Cite this: *Phys. Chem. Chem. Phys.*, 2013, **15**, 3454

Ramzi Farra,*[a] Sabine Wrabetz,[a] Manfred E. Schuster,[a] Eugen Stotz,[a] Neil G. Hamilton,[a] Amol P. Amrute,[b] Javier Pérez-Ramírez,[b] Núria López[c] and Detre Teschner*[a]

CeO_2 has been identified as an efficient catalyst for HCl oxidation in the temperature range of 623–723 K provided that the oxygen content in the feed mixture was sufficiently high to avoid bulk chlorination and thus deactivation. Here we characterise ceria in its fresh and post-reaction states by adsorption of CO_2, NH_3 and CO. Micro-calorimetry, FTIR and TPD experiments are complemented by DFT calculations, which assess adsorption energies and vibrational frequencies. The calculations were performed on the lowest energy surface, CeO_2(111), with perfect termination and with various degrees of hydroxylation and/or chlorination. Both experiments and calculations suggest that the basic character of the ceria surface has been eliminated upon reaction in HCl oxidation, indicating that most of the basic lattice O sites are exchanged by chlorine and that the OH groups formed are rather acidic. The density and the strength of surface acidic functions increased significantly upon reaction. An *in situ* FTIR reaction cell has been designed and constructed to study the evolution of OH group density of the ceria surface during HCl oxidation. The effect of experimental variables, such as pO_2, *p*HCl and temperature, has been investigated. We found that the OH group density positively correlated with the reactivity in the pO_2 and temperature series, whereas negative correlation was observed when *p*HCl was varied. Implications of the above observations to the reaction mechanism are discussed.

Received 8th August 2012,
Accepted 30th December 2012

DOI: 10.1039/c2cp42767b

www.rsc.org/pccp

Introduction

Chlorine is manufactured on the large scale by electrolysis of aqueous NaCl or HCl solutions. The heterogeneously catalysed gas phase HCl oxidation (Deacon reaction) over supported RuO_2 materials offers a viable alternative route to produce Cl_2.[1–7] Despite its recent implementation, the quest for cheaper catalysts led to the recognition of CeO_2 as a highly stable HCl oxidation catalyst.[8] Our performance and characterisation results[8] showed that mildly high-temperature (1173 K) calcined material represents an optimum between stabilised surfaces and unacceptable loss of surface area. The surface of ceria is chlorinated during the reaction and inactive cerium chloride may form when the oxygen over-stoichiometry of the reaction feed is low. As opposed to the metallic nature of RuO_2, ceria requires redox chemistry and thus oxygen vacancies impact the catalytic activity. In a simplified view, the mechanism of Deacon reaction involves reactive HCl adsorption *via* proton abstraction in the formation of OH and surface Cl, recombination of these species (H_2O and Cl_2) and surface re-oxidation by dissociative oxygen activation. It is suggested that several of these steps require an anionic vacancy.

Infrared spectroscopy (FTIR) offers the possibility to characterise surface acid/base properties that can be regarded as a crucial parameter in the adsorption energetics but also in the surface reaction steps of HCl oxidation. Moreover, infrared techniques enable observation of surface species under reaction conditions. *In situ* studies of surface species using FTIR, determination of surface sites and the various cell designs available for these studies have been recently reviewed.[9–11] Ceria is used as a carrier or an additive in various catalytic processes, and *in situ* FTIR has been regularly utilised to extract

[a] *Fritz-Haber-Institute der MPG, Berlin, Germany. E-mail: farra@fhi-berlin.mpg.de, teschner@fhi-berlin.mpg.de; Fax: +49 30 84134676; Tel: +49 30 84135408*
[b] *Institute for Chemical and Bioengineering, Department of Chemistry and Applied Biosciences, ETH Zurich, Wolfgang-Pauli-Strasse 10, CH-8093 Zurich, Switzerland*
[c] *Institute of Chemical Research of Catalonia (ICIQ), Av. Països Catalans, 16, 43007 Tarragona, Spain*

† Electronic supplementary information (ESI) available. See DOI: 10.1039/c2cp42767b

mechanistic details in reactions such as the water–gas shift,[12–15] reverse-WGS,[16,17] low-temperature CO oxidation,[18–20] and PROX.[21,22] *In situ* FTIR studies on ceria as the main catalytic material are, however, much scarcer.[23,24]

In this manuscript, we aim at understanding how the surface acid/base properties of fresh ceria are modified by HCl oxidation. For this purpose, FTIR and micro-calorimetric characterisation of probe molecules (CO_2, NH_3 and CO) in combination with DFT calculations have been applied. Furthermore, we have designed an *in situ* FTIR cell to study ceria under Deacon reaction in the transmission geometry. This cell withstands the corrosive ambient conditions represented by the reaction gas mixture containing HCl, O_2, Cl_2 and H_2O. In the *in situ* experiments we tried to quantify OH groups formed under HCl oxidation and understand their role in the overall mechanism.

Experimental

Sample

Unsupported CeO_2 (Aldrich) was calcined in static air at 1173 K (10 K min^{-1}) for 5 h. This sample, either as fresh (hereafter denoted CeO_2-F) or after Deacon reaction (treated under various feed conditions, ending with HCl : O_2 = 1 : 9 at 593 K, hereafter denoted CeO_2-D) was used for characterisations.

HRTEM characterisation

High resolution transmission microscopy with aberration correction (FEI Titan Cs 800–300) was utilised to assess the morphology of the ceria particles.

NH_3 temperature programmed desorption

NH_3-TPD was measured in a Thermo TPDRO 1100 unit equipped with a thermal conductivity detector. The samples (300 mg) were loaded in the quartz micro-reactor (11 mm i.d.), pre-treated in He (20 cm^3 STP per min) at 573 K for 3 h, and cooled to 373 K in He. NH_3 was chemisorbed at 373 K in three consecutive cycles of saturation with 10 vol% NH_3/He (20 cm^3 STP per min) for 30 min followed by purging with He (20 cm^3 STP per min) at the same temperature for 30 min. Desorption of NH_3 was monitored in the range of 323–1273 K using a heating rate of 20 K min^{-1} and a He flow of 20 cm^3 STP per min.

Micro-calorimetry

Micro-calorimetric experiments were carried out in a Calvet calorimeter (SETARAM MS70) combined with a high vacuum system, which enables the dosage of probe molecules within a range of 0.02 μmol. The samples were pre-treated according to the following procedure: CeO_2-F was exposed to synthetic air at 773 K for 5 h, whereas CeO_2-D (after Deacon) was only degassed under UHV at 423 K for 5 h. The pre-treatment was conducted in a separate chamber connected to the calorimetric cell. The final pressure in the degassed cell was approximately 10^{-6} mbar. The cell was cooled to room temperature, placed inside the calorimeter, and connected to the micro-calorimetric gas-adsorption system. Subsequently, CO_2 or NH_3 was dosed stepwise at 313 K. Pressure, adsorption temperature, and the heat signals were recorded during all dosing and desorption steps. Desorption was performed at adsorption temperature under UHV. In all calorimetric sections positive energy corresponds to an exothermic process.

Probe molecule adsorption by FTIR

Fourier transform infrared (FTIR) spectroscopic measurements were carried out using a Perkin-Elmer Pe100 spectrometer equipped with an MCT detector. The spectra were recorded with a resolution of 2 cm^{-1} and accumulation of 64 scans. Self-supported wafers were prepared by pressing the sample under a pressure of 230 bar. The samples were activated first *in situ* prior to IR measurements. The cell is connected to a vacuum system with a residual pressure of *ca.* 1×10^{-7} mbar. A background spectrum of the empty cell was used to subtract the CO adsorption spectra of the sample. CO was initially dosed at 77 K up to equilibrium pressure (1.86 mbar for non-chlorinated and 1.31 mbar for chlorinated ceria). Then, the gas was evacuated in sequential steps in order to study the coverage dependence.

In situ FTIR in HCl oxidation

An *in situ* transmission FTIR cell (Fig. 1) has been designed to enable investigating Deacon catalysts under reaction conditions. Details of the cell design will be discussed in the Results section. A CeO_2-F sample was pressed into a self-supporting disc (31.8 mg cm^{-2}) and placed in the sample holder in the center of the furnace of the IR cell. The sample was heated in flowing synthetic air up to 723 K (10 K min^{-1}) and allowed to stabilise for 90 min. Spectra were recorded using a Varian-670 FTIR spectrometer under the reaction conditions indicated. A resolution of 4.0 cm^{-1} was used throughout the investigation and in most cases 512 scans were averaged to achieve a satisfactory signal-to-noise ratio. Reactivity was followed by means of iodometric titration. Reaction feed, at constant 100 cm^3 STP per min total flow, was supplied by mass flow controllers. The Deacon reaction was started in an oxygen-rich atmosphere with a feed composition HCl : O_2 : N_2 = 1 : 9 : 0 at 703 K. The reaction was maintained under this condition for 16 h before starting to investigate the effects of various reaction conditions (p_i, T). During the O_2 partial pressure dependence, the HCl flow was kept constant at 10 cm^3 STP per min and the O_2 flow was varied according to the following feed composition sequence: HCl : O_2 : N_2 = 1 : 9 : 0, 1 : 4 : 5, 1 : 2 : 7, 1 : 1 : 8 and 1 : 0.5 : 8.5. During the measurement of HCl partial pressure dependence, the O_2 flow was kept constant at 20 cm^3 STP per min and the HCl flow was changed as follows: 10, 6, 3 and 1 cm^3 STP per min. The time interval for each of the above steps was ~5 h, and the temperature was kept constant at 703 K. The temperature effect was studied at an oxygen-rich feed composition of HCl : O_2 : N_2 = 1 : 9 : 0 by reducing the temperature, stepwise by 20 K, starting from 703 K and ending at 623 K. The time interval for each step was ~4 h.

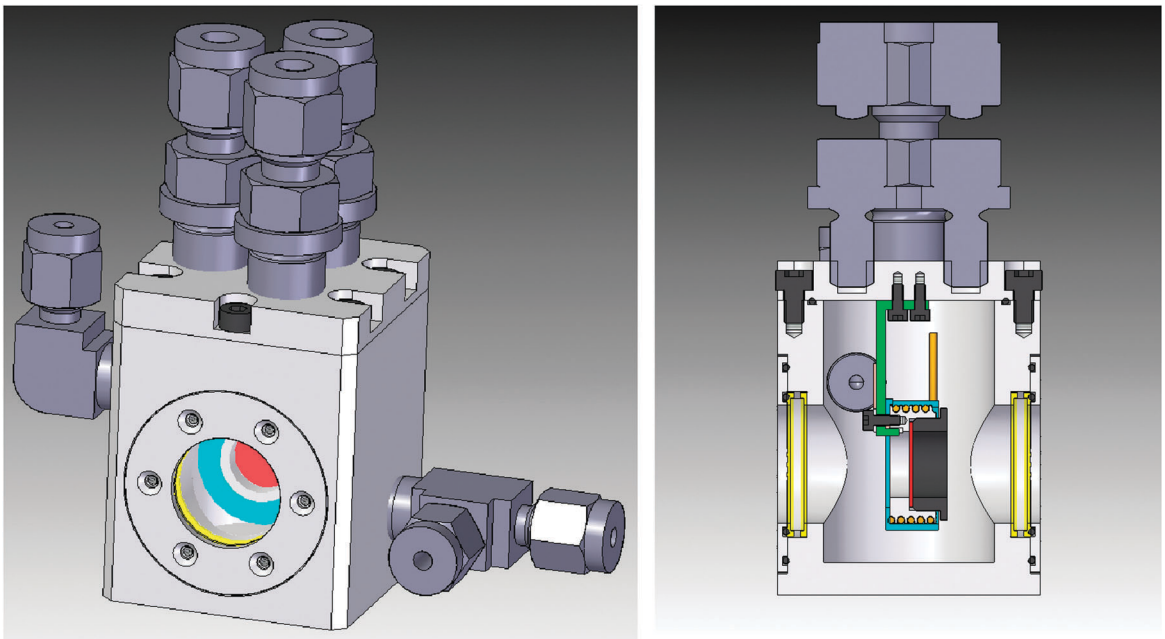

Fig. 1 Scheme of the *in situ* FTIR cell with gas inlet and outlet at the sides and three feedthroughs at the top (2 for thermocouples and one for heating). The investigated sample (red in the online version) is held in a heatable stage.

Density functional theory calculations of probe molecule adsorption

Density functional theory (DFT) simulations have been applied to CeO_2 slabs. The calculations were performed with the 5.2.12 version of the VASP code.[25] The functional of choice was PBE+U,[26] to partially account for self-interaction issues in the f-electrons. The U parameter chosen was set to 4.5.[27–29] Inner electrons were replaced by PAW pseudopotentials[30] while the 12 valence electrons of Ce atoms in the 5s, 5p, 6s, 4f, 5d states and the 6 valence electrons of O atoms were considered explicitly. The valence electrons were expanded in plane waves with a cut off energy of 400 eV. For further details the reader is referred to ref. 8. The lowest energy surface, $CeO_2(111)$, was taken as representative of the material. The chosen slab corresponds to a $p(2 \times 2)$ reconstruction and contains 3 layers. The k-point sampling was set to $5 \times 5 \times 1$.[31] Slabs were interleaved by 10 Å and artificial polarisation interactions due to the asymmetry of the adsorption configuration were removed by standard procedures. Spin polarised calculations were performed when needed. Vibrational frequencies were calculated through the diagonalisation of the numerical Hessian obtained by displacements of ± 0.02 Å for each degree of freedom. A description of how good theoretical methods are at analysing acid–base properties of surfaces can be found elsewhere.[32] The full tables with adsorption energy and frequency calculations and spin states are presented in the ESI† and only the most representative features are described in the main text.

Results and discussion

HRTEM

HRTEM analysis of the CeO_2-F sample mostly revealed well faceted particles in the range of 20–50 nm with a few larger particles around 100 nm (Fig. 2). Many particles show (111) lattice fringes with a well faceted surface, suggesting the formation of energetically stable surface orientations. The sample after 80 h in the Deacon reaction revealed some changes in the morphology of the particles. The overview micrographs show the relatively broad particle size distribution being conserved, though many of the sharp corners of the CeO_2 particles seem to be smoothed and rounded upon the reaction. Despite the smoothening of edges, the crystalline structure remains that of CeO_2.

Micro-calorimetry and corresponding DFT analysis

The pressure-controlled dosing system of the calorimeter with calibrated volume enables the quantification of adsorbed molecules (adsorption isotherm) as well as the differential heat of adsorption and gives the possibility to elucidate the distribution of the adsorption sites along the range of adsorption heats. These results (Fig. 3) are compared with the modelling obtained through DFT in order to unravel the nature of the adsorption sites.

It has been shown that the Deacon reaction gives rise to surface chlorination,[8] thus, it is expected that acid–base properties of the surface are modified. Ceria is an amphoteric compound showing both surface acidity and basicity. Therefore, NH_3 and CO_2 probe molecules were used to assess acidic and basic properties of the samples, respectively, before and after reaction. For comparison, calculations were performed on different models representing the local structures in Fig. 4. Adsorption of probe molecules using DFT calculations has been performed on a model CeO_2 (111) surface and with different degrees of hydroxylation and/or defects involved, Fig. 4 (For the configurations with adsorbates see Fig. S1, ESI.†). Finally, a summary with the

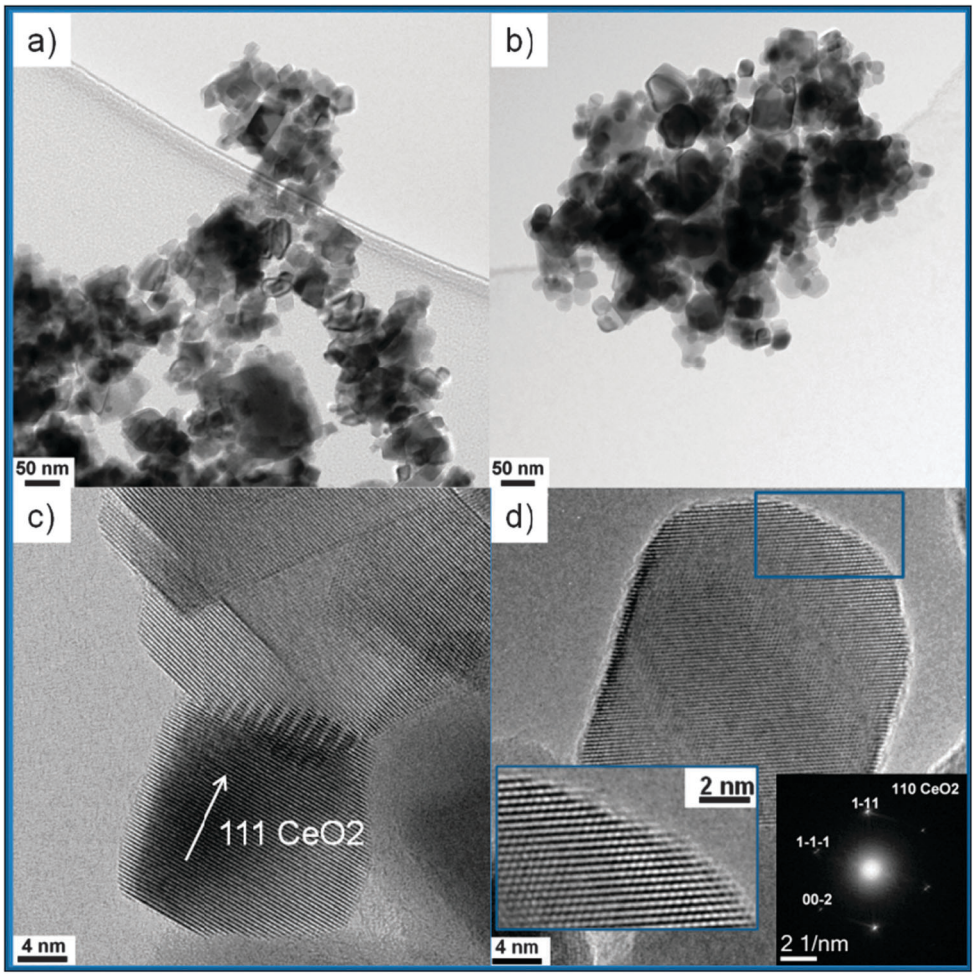

Fig. 2 TEM and HRTEM comparison of CeO_2 before (a and c) and after Deacon reaction (b and d). The sample after reaction was taken from the pellet used for the *in situ* FTIR experiments.

assignments based on either adsorption energies or frequencies is proposed (Table 1).

CO_2 adsorption was performed at 313 K in order to derive information from the pure adsorption process by suppressing secondary reactions, which have been shown to occur at higher temperatures.[33] The results are depicted in Fig. 3A and B. The differential heat of adsorption profile as a function of CO_2 uptake for the CeO_2-F demonstrates energetically wide distribution of basic interacting sites. Nevertheless, two distinct sites exhibited uniformity, as can be recognised by two plateaus at very low and relatively high pressures (Fig. 3B). The amount of these two energetically homogeneous sites (*ca.* 7 μmol g^{-1} CO_2 adsorbed for each plateau) is small in comparison to the whole available basic sites on the surface. The initial heat of adsorption is about 110 kJ mol^{-1}. These adsorption energies were suggested to correspond to structural defects such as edges in nanoparticles[34] or vacancies in more open facets such as (110).[35] In our calculations, multiple (3) CO_2 adsorption on a single vacancy site could account for a large average adsorption energy >100 kJ mol^{-1} (see Table S3, ESI†). The adsorption energy profile in Fig. 3B decreases gradually with coverage until reaching the second plateau at about 55 kJ mol^{-1}. This energy plateau can be assigned to the formation of carbonate species (our calculation: 43 kJ mol^{-1}) with the basic O atoms on the surface (Fig. S1(i), ESI†). In Fig. 3B, a small amount of CO_2 adsorbed with lower heat of adsorption values. Indeed, the calculations show that the interaction with partially hydroxylated surfaces is weaker (18 kJ mol^{-1} and lower) and similar values are retrieved for oxygen vacancies when one of the O atoms of the CO_2 molecule fills the vacancy. Repeated adsorption experiment after desorption (at 313 K, UHV) revealed a certain degree of irreversible adsorption; either related to strong adsorption on low coordination sites and/or carbonate formation. The decrease of the heat of adsorption at the first plateau may be explained by the repulsive interaction of CO_2 with the irreversibly adsorbed species. By considering the wide range of heats of adsorption, it can be conveniently concluded that both Lewis and Brønsted basic sites are present in the non-chlorinated sample.

In contrast to CeO_2-F, CO_2 does not show any considerable interaction with the chlorinated surface, even at relatively high CO_2 pressures (Fig. 3A). Indeed, very weak adsorption energies were calculated on the models for the partially chlorinated

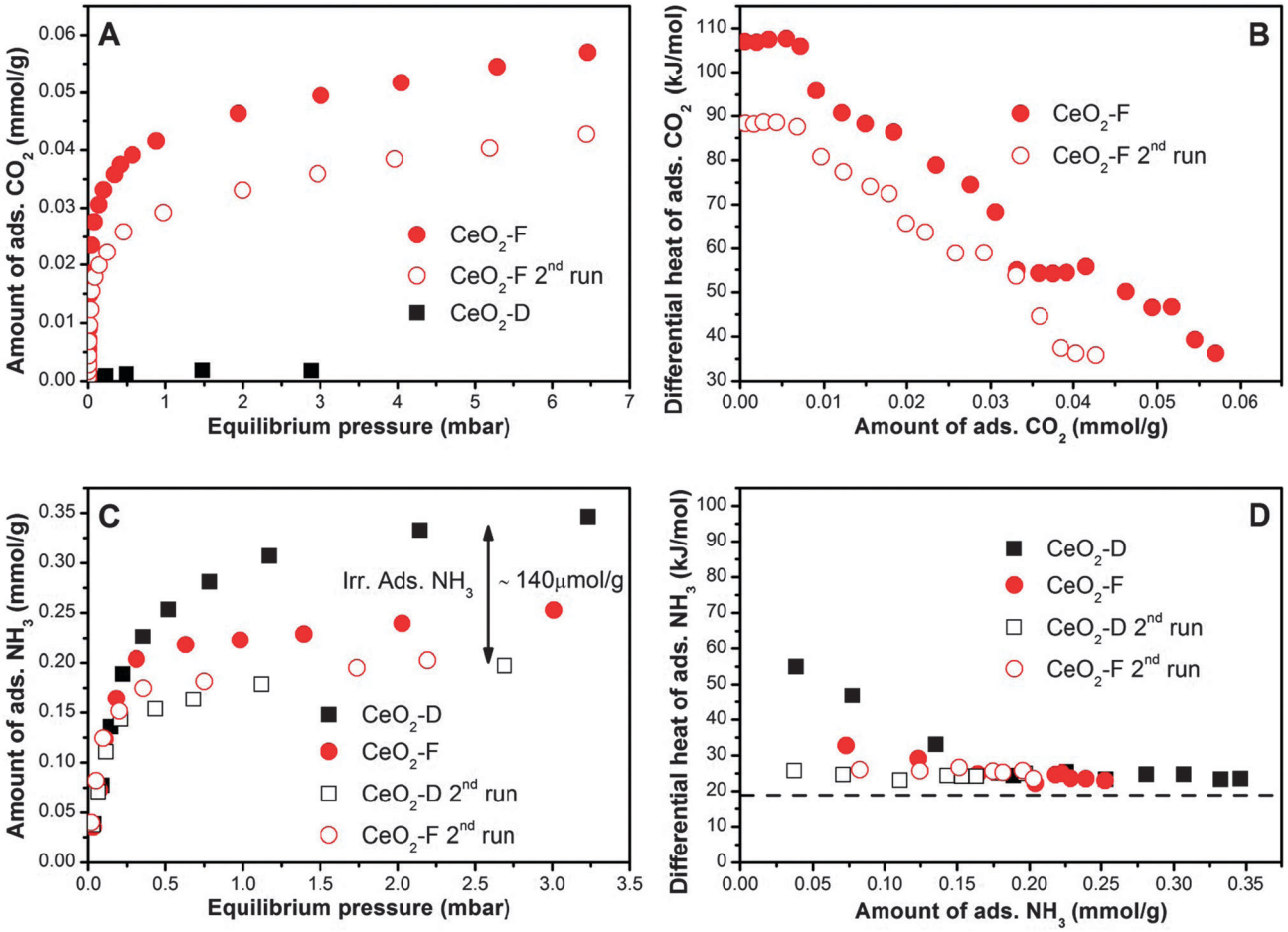

Fig. 3 Adsorption isotherms (A and C) and differential heat of adsorption data of CO_2 (A and B) and NH_3 (C and D) on fresh and post Deacon CeO_2 studied by microcalorimetry. When indicated, a 2nd adsorption was carried out after desorption under UHV. T = 313 K.

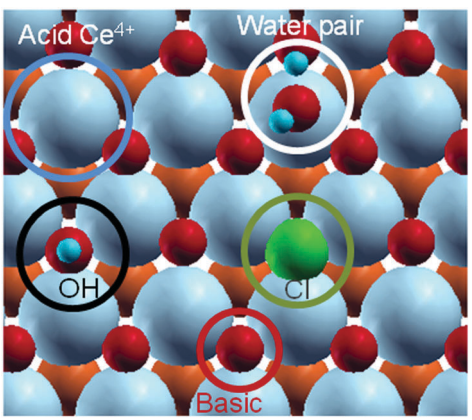

Fig. 4 Schematic representation of adsorption sites on the CeO_2(111) surface. The different sites are highlighted by the circles. Light blue spheres represent Ce atoms, orange sub-surface O atoms, red O, green Cl and white H. CeO_2H ($O_{lattice}H$) corresponds to the OH group on the left and CeO_2H–OH is the water pair. Colour applies for the online version.

surfaces (see Table S3, ESI†). Therefore, we can confidently infer that during the reaction CeO_2 lost basicity due to surface chlorination and acidic hydroxyl formation (detailed in later sections). In other words, the population of Lewis sites seems to be greatly attenuated[36] and that of Brønsted sites (OH groups) does not possess basic properties anymore.

NH_3 was employed to investigate acidic properties of the samples. Due to stainless steel tubing applied in our microcalorimetric setup, the determination of the initial differential heat of adsorption values was not straightforward. Hence, initial values at very low NH_3 pressures were not analysed. The ammonia adsorption results are illustrated in Fig. 3C and D. The chlorinated sample gave rise to enhanced interaction up to $\sim$150 μmol g^{-1} adsorption, after which both samples reach a plateau at $\sim$25 kJ mol^{-1}. The isotherm and heat of adsorption values demonstrate an increased acidity of the chlorinated surface. Re-adsorption evidences a significantly higher amount ($\sim 3\times$) of irreversibly held ammonia on the sample after Deacon reaction. The concomitant presence of high proton density, leading to a larger number of NH_4^+ groups, and high polarisability of the chlorine atoms on the surface that increases the electrostatic interactions can be responsible for the enhanced ammonia adsorption in the post-reaction sample.

Table 1 Summary of the experimental and calculated adsorption, E in kJ mol^{-1}, and vibrational frequencies, ν in cm^{-1}, of probe molecules together with the corresponding model

Molecule	E^{exp}	ν^{exp}	E^{calc}	ν^{calc}	Species	Model
CO_2	110				CO_3^{2-}	Multiple adsorption at vacancies
	55		43		CO_3^{2-}	Regular surf.
NH_3	—	1394	—	1416–1382	NH_4^+	Brønsted
	—	1557	50	1593–1566	NH_3/NH_4^+	Lewis
	—	1414		1615–1612	NH_4^+	Chlorinated surface
CO	—	2155		2112		($O_{lattice}H$)
	—	2161		2127		($O_{lattice}H\cdots OH$) chlorinated
	—	2186		2157		($O_{lattice}H\cdots Cl$)

FTIR spectra for ammonia adsorption on fresh and chlorinated samples (not shown) also reveal a stronger interaction of NH_3 with the chlorinated sample, as the peaks that are believed to correspond to the interaction with Brønsted (1396 cm^{-1}) and Lewis (1557 cm^{-1})[37] acid sites are both shifted to the higher frequencies in this case. This is indeed seen from the calculations as the direct interaction to Ce^{4+} sites is calculated to give a main peak at 1593 cm^{-1}, which shifted upon chlorination to 1615–1612 cm^{-1}. Other bands in the same region may correspond to NH_3 adsorption to hydroxyl groups on the surface, 1566, 1562 (CeO_2H) and 1583 cm^{-1} (CeO_2H–OH).

The acid strength distribution on the CeO_2 samples related to the *irreversible* NH_3 adsorption in the micro-calorimetry was studied further by NH_3-TPD in the range of 323–1273 K (Fig. 5). The distribution of acid sites on the fresh CeO_2 is broad, indicating the presence of both medium and strong acid sites. The medium acid sites appear to be much more abundant than strong ones. These results are in good agreement with the previous literature reporting on the acidity/basicity of rare-earth oxides.[38] For the CeO_2-D sample a new TPD peak centered at *ca.* 555 K and a large peak in the broad range of 800–1000 K appeared. These peaks cannot be due to chlorine desorption from the catalyst surface as the TGA-MS analysis showed a very small amount of chlorine leaving the surface (in the range of 500–660 K, Fig. S2, ESI†). Accordingly, these peaks are attributed to the generation of new medium and strong acid sites during HCl oxidation. Integration of the TDS signal yields an approximately 3-times higher response for the CeO_2-D sample in good agreement with the observed ratio of irreversible NH_3 adsorption by microcalorimetry (see Fig. 3C).

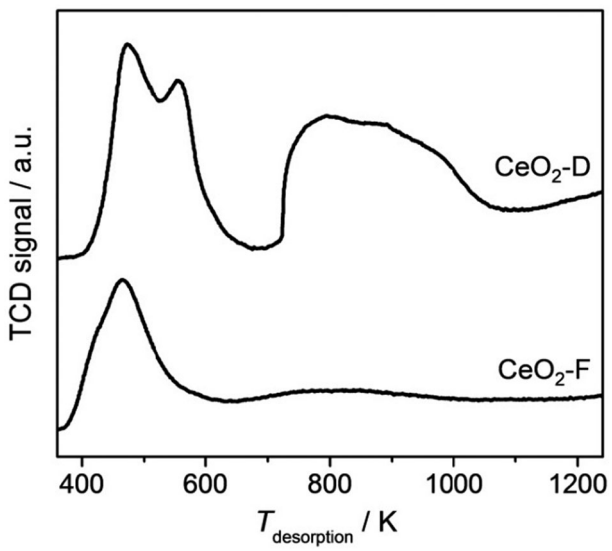

Fig. 5 NH_3-TPD profiles of fresh and post Deacon CeO_2 samples.

When comparing to the computed results, within the PBE+U approach, the adsorption of ammonia with the N-down configuration on the Ce^{4+} site of the undefective surface is 50 kJ mol^{-1} (see Fig. S1(e), ESI†). (A second configuration with the three H atoms interacting with 3 neighbouring Lewis basic sites, *i.e.* O anions, leads to mere 9 kJ mol^{-1}.) Adsorbed on Brønsted acids (OH models), the adsorption is slightly weaker (31–39 kJ mol^{-1}). Using the model with partial chlorination and concomitant neighbouring Brønsted (OH) sites on the surface the interaction is stronger (about 60 kJ mol^{-1}) in agreement with the experimental observations. These values are somehow smaller than the 500 K desorption peak would indicate, but they will be largely affected by the coordination of the Ce^{4+} cations. It is likely that the structure at higher desorption temperatures found in TPD arises from breaking the NH_4^+ binding to the surface (see Table S2, ESI† for the configurations). With surface hydroxylation two different configurations may exist: one with $OH\cdots NH_3$ interactions, where the H is still bonded to oxygen on the surface, or ammonia can strip the H from some of these centers to generate NH_4^+ species that can wander on the surface (see *e.g.* Fig. S1(g), ESI†). Electrostatic interaction of NH_4^+ with polarised surface Cl will further strengthen ammonia adsorption. The elimination of this species in the form of ammonia likely requires more energy than any other NH_3 desorption process, but it is unfortunately not well-reproduced by the calculations due to the charge displacement, the total charge state and the periodic boundary conditions employed in the simulations.

Probe molecule adsorption by FTIR and corresponding DFT analysis

CO is one of the most frequently used probe molecules in IR spectroscopy. Owing to its specific properties (sensitivity, accessibility and high extinction coefficient) crucial information can be obtained in terms of identification of adsorbing sites (Brønsted and Lewis) and definition of oxidation states.[39] In comparison to experiments, the DFT calculations underestimate the CO stretching frequency and thus only shifts are usually discussed to analyse

the results. It is worthwhile mentioning here that the σ-bond and electrostatic interactions cause hypsochromic frequency shifts, and the electrical field strength of metal ions is not only dependent on the formal charge but also the contribution of the metal ions' environment to the effective charge must be taken into account.[39] Hence, the effect of surface chlorination on the acid–base properties was further studied by monitoring shifts of CO vibrational frequencies at 77 K on both fresh and chlorinated samples. The former was pre-treated in batch at 200 mbar oxygen and 823 K for 5 h, O_2 had been replaced every 30 min to prevent re-adsorption of desorbing contaminants. The chlorinated sample was pre-treated in O_2 (200 mbar) at only 473 K for 5 h, as the surface after chlorination and thus replacement of O^{2-} anions is now less prone to the formation of carbonate species.[36] Further, this minimises dechlorination. The samples were subsequently evacuated during cooling down. CO adsorption spectra on CeO_2-F are shown in Fig. 6a. After equilibration with 1.86 mbar CO at 77 K, two close and overlapping peaks at 2150 and 2155 cm^{-1} with two shoulders at 2172 and 2140 cm^{-1} appeared.

Taking the IR frequency of gas phase CO (2143 cm^{-1}) as a reference, we can attribute the aforementioned bands and shoulders as follows: (i) the shoulder at 2140 cm^{-1} can be assigned to the physisorbed CO, since it is the closest one to the reference value, and it desorbs easily upon evacuation, (ii) the bands at 2150 and 2155 cm^{-1}, which are slightly up-shifted, can be attributed to CO hydrogen-bonded to OH groups of different acid strengths. This carbonyl band is accompanied by intensity perturbation and redshift of the ν(OH) bands (see the inset in Fig. 6a). Further evacuation gives rise to the disappearance of the band at 2150 cm^{-1}, which seems to have weaker interaction with the surface OH groups, whereas the band at 2155 cm^{-1} was decreasing gradually and shifting to higher wavenumbers with increasing vacuum. This shift is attributed to the diminishing intermolecular interactions at lower coverage.[40] By considering CO as a weak electron donor molecule, the higher the positive shift of Δ(CO), the stronger is the interaction with surface sites. The minor shoulder at 2172 cm^{-1} can be assigned to the CO interaction with Ce^{4+} sites,[41,42] in agreement with the stronger adsorption of CO on the cationic site. However, DFT adsorption energies on cus Ce^{4+} is mere 18 kJ mol^{-1}, and therefore this band is more likely related to adsorption on more open surface sites.

Calculations are not fully conclusive at this stage. Indeed, adsorption energies have previously been calculated with different approximations leading to a range of 16–25 kJ mol^{-1},[43] and the presence of hydroxyl groups, although induces CO shifts of +40 cm^{-1}, reduces the adsorption energy further ($O_{lattice}H$ model). Partially water covered surfaces (the CeO_2H–OH water pair model) might be responsible for stronger adsorption, about 48 kJ mol^{-1}, with the CO shift being dependent on the type of surface site (lattice or on top OH) CO interacting with (see Table S4, ESI†). The frequency shift is about +10 cm^{-1} when adsorption takes place close to the Ce^{4+} cations.

FTIR spectra of CO adsorption on chlorinated sample are illustrated in Fig. 6b. The main peak at high coverage is situated at 2161 cm^{-1}. According to the calculations this can be assigned to CO interacting with hydroxyls on the surface where the CO molecule is basically sitting with the C-down close to a Ce atom (see Fig. S1(o), ESI†). As these sites are not blocked in the Deacon reaction they seem to be rather stable when compared to the clean surface. There is an additional shoulder at 2144 cm^{-1} and a small band at 2186 cm^{-1}. Upon evacuation, the band at 2144 cm^{-1}, which is very close to the gas phase ν(CO) disappeared. At lower pressures, the intensity of the main band further decreases and shifts to the higher wavenumber and splits up into two peaks. All bands, with exception of physisorbed CO at 2144 cm^{-1}, are blue shifted by ~10 cm^{-1} in comparison with those from the non-chlorinated sample. This blue shift indicates an overall increase of the acidity of the surface upon chlorination. The extent of the redshift of the OH band upon interaction with CO (inset in Fig. 6a) has often been utilised to evaluate the strength of surface Brønsted acid sites.[39,40,44–46] The magnitude of OH

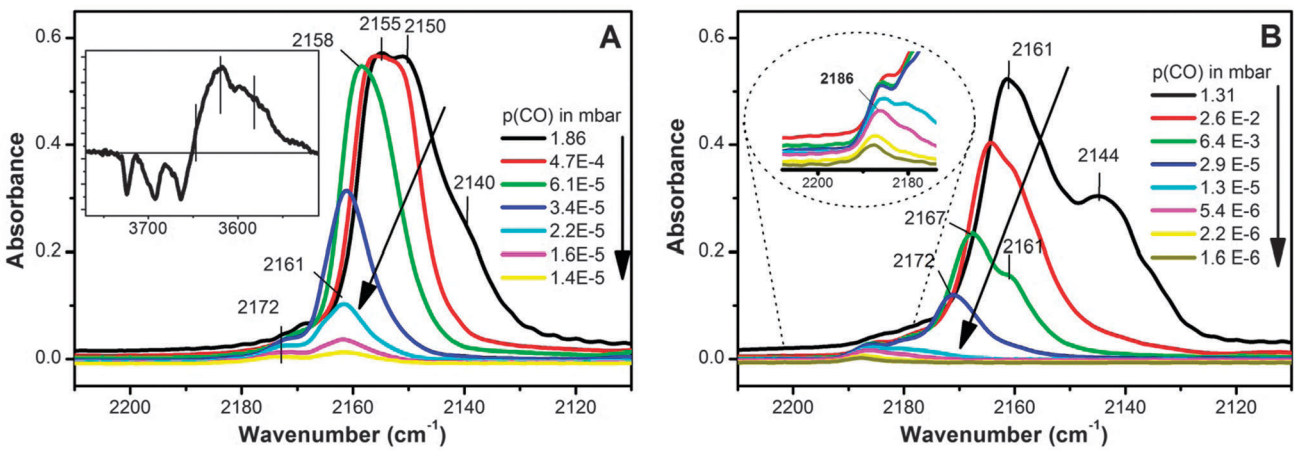

Fig. 6 (A) FTIR spectra of CO adsorbed at 77 K on fresh CeO_2; after admission of 1.860 mbar CO in equilibrium (black-spectrum), after various sequential steps of evacuation (rest). Inset: the difference spectrum of the sample before and after admission of CO; (B) FTIR spectra of CO adsorbed at 77 K on CeO_2-D; after admission of 1.306 mbar CO in equilibrium (black-spectrum), after sequential steps of evacuation (rest). Inset: zoom in for the band at 2186 cm^{-1}.

shifts was ~75 cm^{-1} for the fresh CeO_2. The calculated value for CO-induced shifts of $O_{lattice}H$ is about 100 cm^{-1}. Whereas, it is in the range between 137 and 164 cm^{-1} for ceria after Deacon reaction, corroborating the enhanced acidity of the Brønsted sites. This latter value is not reproduced in the calculations and one of the reasons for the discrepancy might be high surface water content.

In situ FTIR under Deacon reaction

Cell design. For a successful *in situ* cell design, several aspects should be taken into consideration, such as small void volume, suitable IR-windows and construction materials, especially when it comes to such highly corrosive gaseous conditions, as for the Deacon reaction.

Our cell (Fig. 1) consists of two main parts. The cell body is provided with two IR transparent Si windows and two 1/8 in. tubing for the inlet and outlet of the reactant gases and products. Si windows (20 mm id, 1 mm thickness) were fixed between two PTFE gaskets and sealed with Kalrez o-rings, which are chemically resistant at relatively high temperatures. The body of the cell is made of stainless steel; however a galvanic silver coating was applied on the inner walls. Silver is resistant to dry and moist chlorine at room temperature. A compact film of silver chloride is expected to form during the exposure of silver to molecular chlorine. This chloride layer is responsible for the resistance of the silver.[47]

The lid is provided with a cylindrical oven (sample holder) and thermocouple for monitoring the temperature of the sample. Hastelloy C-22 was used as constructing material for the lid, which is coated afterwards with a special inert Si-based coating (Silcolloy™ 1000) using the CVD procedure. The sample holder serves as the heating system that operates in the temperature range from 300 to 823 K. The internal volume of the cell is *ca.* 20 cm^3.

***In situ* experiments.** It has been proposed recently[8] that the mechanism of the Deacon reaction on CeO_2 includes two elementary steps that describe the formation and consumption of OH groups during the reaction. These results were based on DFT calculations. IR spectroscopy is among the best spectroscopic techniques known for monitoring the changes of OH groups under reaction conditions. Therefore, *in situ* IR experiments were carried out at different feed compositions and temperatures in the hope that mechanistic information could be extracted and to correlate the abundance of OH species with the catalytic activity of the sample.

CeO_2-F was activated *in situ* by heating in synthetic air up to 703 K and holding at this temperature for 90 min. Two main bands were observed at the end of this stage at 3700 and 3620 cm^{-1}, which are assigned, respectively, to mono-coordinated (OH-I) and bridging (OH-IIB) OH, see Table S1 (ESI†).[48] In our recent work with ceria calcined at only 773 K, these bands were slightly shifted to higher frequencies (*ca.* 10 cm^{-1}) and the band at 3730 cm^{-1}, which was considered as a shoulder, is better resolved now. Our current sample was calcined at higher temperature (1173 K), which results in a decreased density of the OH groups as well as a better Deacon performance despite the lower BET surface area.[8]

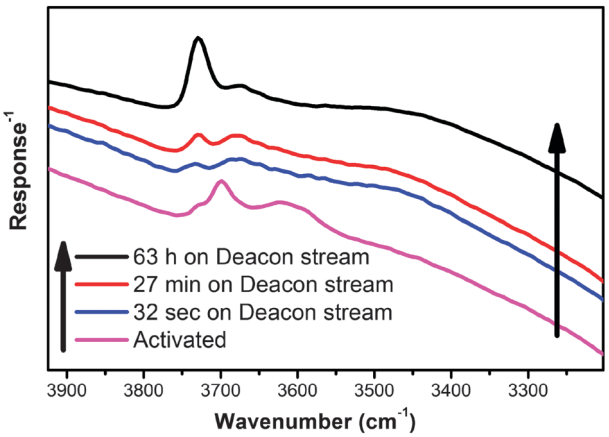

Fig. 7 *In situ* single beam FTIR spectra of CeO_2 under various conditions: activated (before HCl introduction) and in Deacon reaction.

HCl was introduced in the feed ratio HCl : O_2 = 1 : 9 at 703 K. Similar changes (Fig. 7) were observed at the early stages of the reaction as with the lower temperature calcined CeO_2 and strongly diluted Deacon feed.[8] Both OH bands at 3621 and 3700 cm^{-1} have vanished upon HCl introduction, the band at 3730 cm^{-1} was better resolved, and a broad band near 3500 cm^{-1} developed. This latter is related to surface water.[8,49] A pronounced increase of the band at 3730 cm^{-1} was observed in advanced stages of the reaction (see Fig. 7, black spectrum), whereas another low intensity band at 3676 cm^{-1}, which is observed only after introducing HCl into the feed, does not show remarkable variation with time. Since the initial changes under Deacon conditions were very fast, the single beam spectrum after 32 s on the Deacon feed (blue spectrum) was used as background to follow the evolution of the band at 3730 cm^{-1}. The time evolution of absorbance spectra was fitted (see Fig. S3, ESI† as an example) and we analyse the evolution of the abundance of the mono-coordinated OH component. The integral area of this peak at 3730 cm^{-1} increased very rapidly at the beginning of the reaction (Fig. 8). Then, changes slowed down appreciably, though no plateau was reached even after 16 h on stream. This phenomenon may be interpreted based on structural evolution of the surface during the reaction, with sharp facets becoming more rounded. This morphological transformation may require the extended time experienced in the IR experiment.

The reaction conditions (p_i and T) were varied individually to study the influence of each parameter on the concentration of the OH groups. Fig. 8 shows the integration data for the whole experiment, in which first pO_2, then pHCl and lastly temperature was varied. Due to the non-steady nature of OH even after 16 h, we repeated the same reaction conditions twice to control the effect related to this. These data were fitted with a mathematical function and the actual OH abundance has been corrected with the hypothetical value given by the fit at the corresponding time on stream.

O_2 dependence. The effect of various pO_2 contents in the feed on the reaction rate level and the OH concentration compared

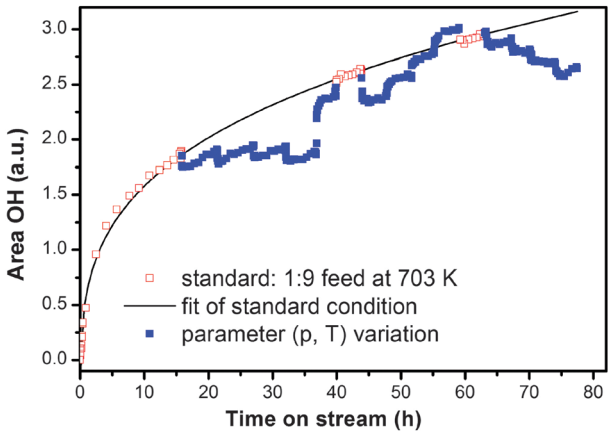

Fig. 8 Evolution of integrated area of the OH band at 3730 cm^{-1} as a function of time on the Deacon stream. Red points represent the standard conditions of HCl : O_2 = 1 : 9 at 703 K and the black line is a fit to these data. Blue points represent various other conditions in the Deacon feed during pO_2, *p*HCl and *T* variation. These are discussed in detail in Fig. 9–11.

to that in the standard feed of HCl : O_2 = 1 : 9 is illustrated in Fig. 9. Increasing oxygen content gives rise to increasing reactivity that can be fitted to a formal pO_2 dependence of ~0.4. In parallel, the OH concentration is the highest at the most oxygen rich feed and decreases continuously when pO_2 is lowered. The major changes in the OH concentration occur fast, usually within 2–3 min, thus the surface rapidly responds to the changes in the feed stream. In this experiment we observe a positive relationship between OH concentration and the reactivity, in the sense that higher OH coverage results in higher conversion.

HCl dependence. Before starting the investigation of *p*HCl dependence, the sample was reactivated by switching to O_2 rich feed compositions (HCl : O_2 = 1 : 4 then 1 : 9, 3 h for each), since feeds with low oxygen content were shown to induce deactivation.[8]

According to the proposed mechanism,[8] HCl dissociation on the surface is a fundamental reaction step, which is responsible for the compensation of OH group's loss during the formation of the by-product H_2O. Thus, one may assume that by reducing the inlet *p*HCl, OH concentration will decrease. Fig. 10 demonstrates exactly the opposite behaviour, that is, by reducing *p*HCl (from 10 to 1 cm^3 STP per min in always constant 100 cm^3 STP per min total flow) and keeping also pO_2 constant (20 cm^3 STP per min), OH concentration has steadily increased. In parallel, the Cl_2 productivity decreased, and therefore in this experiment the higher reaction rate correlates with decreasing OH concentration.

T dependence. Temperature influence was studied by reducing the temperature stepwise (20 K for each step) in the range from 703 to 623 K. Decreasing reaction temperature induces a loss of activity according to the Arrhenius law. The calculated apparent activation energy is 70 kJ mol^{-1}. Fig. 11b indicates that decreasing temperature and reactivity correlates with lower OH concentration, similar to that found in pO_2 dependence.

Mechanistic considerations. Micro-calorimetric experiments with CO_2 adsorption suggested a loss of basic character of the ceria surface after reaction under Deacon conditions. That is, most of the basic lattice O surface sites are exchanged to surface (lattice) Cl and the OH groups are no more Lewis basic, but rather Brønsted acidic. Surface chlorination is in line with our previous XPS characterisation.[8] H abstraction during dissociative HCl adsorption requires basic sites, and hence HCl adsorption is certainly retarded by the loss of basic character. Ammonia and CO adsorption studies by micro-calorimetry, FTIR, and TPD, confirmed the increase in the acidic character after Deacon reaction, at likely both the cus Ce^{4+} and OH positions. The calculated adsorption energies and vibrational frequencies by DFT were, generally, in accordance with the experiments. Due to the lack of other surface orientations considered and the partial sampling of potential defects, the DFT picture of CO and CO_2 adsorption and agreement to

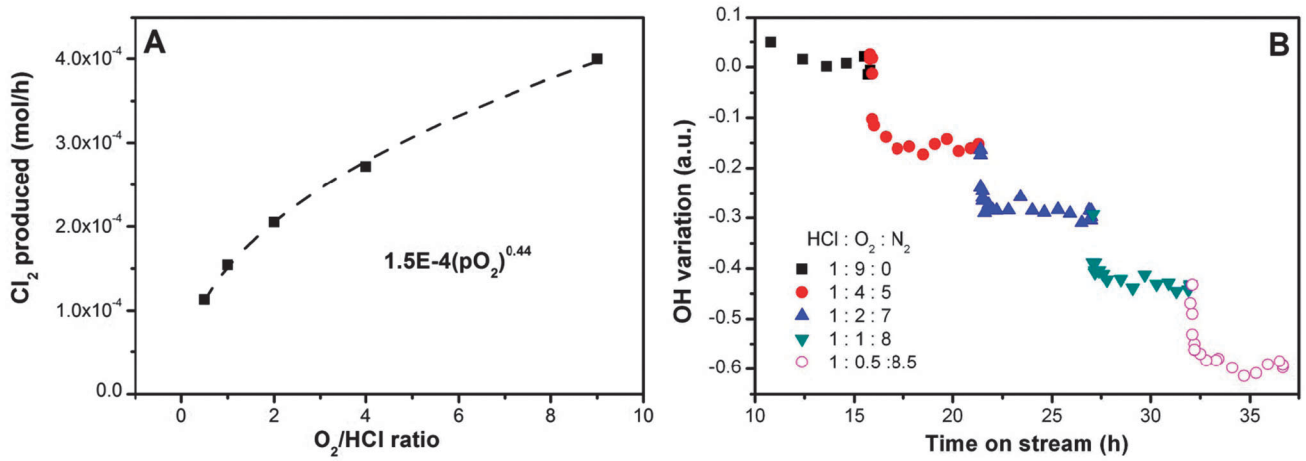

Fig. 9 *In situ* results at 703 K during pO_2 variation. (A) Conversion as a function of O_2 content of the feed. (B) Evolution of integrated OH area as a function of time on the Deacon stream during pO_2 variation. OH variation is expressed as the difference of the OH area at 1 : 9 : 0 feed according to the fit at the corresponding time on stream and the actual measured area.

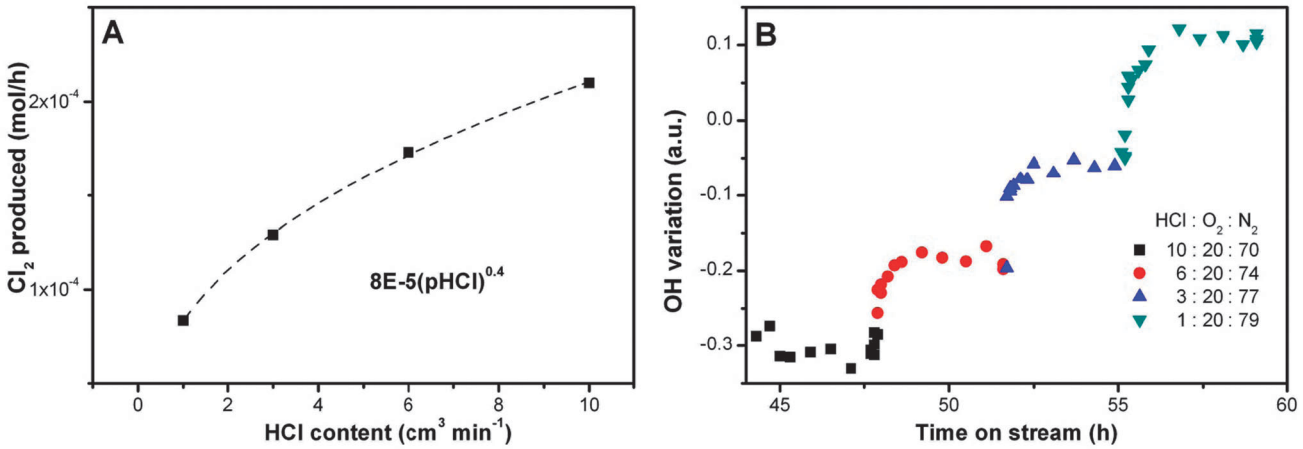

Fig. 10 *In situ* results at 703 K during *p*HCl variation. (A) Conversion as a function of HCl content of the oxygen-rich feed. (B) Evolution of integrated OH area as a function of time on the Deacon stream during *p*HCl variation. OH variation is expressed as the difference of the OH area at 1 : 9 : 0 feed according to the fit at the corresponding time on stream and the actual measured area.

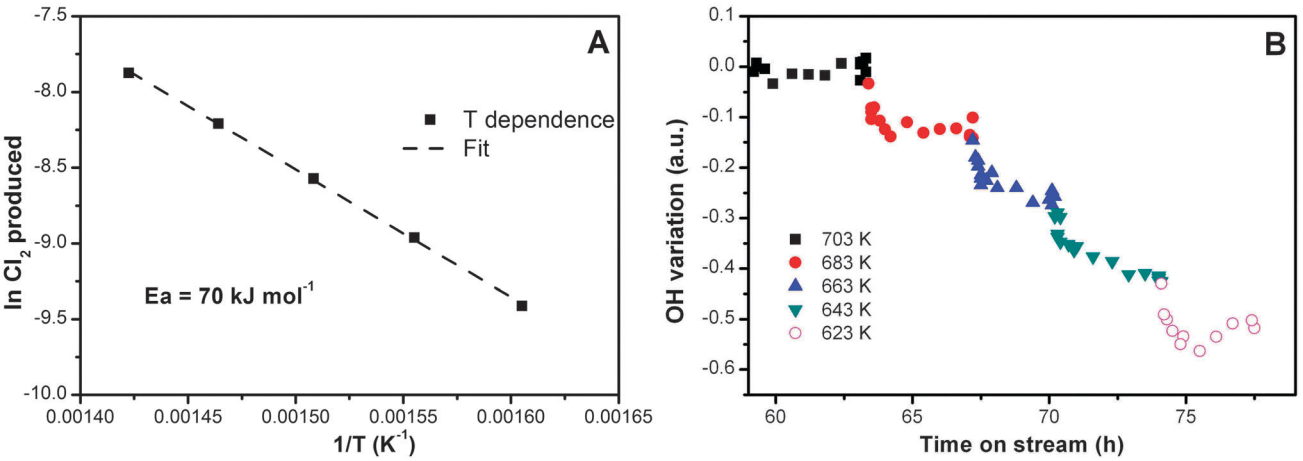

Fig. 11 *In situ* results during temperature variation using a feed of HCl : O_2 : N_2 = 1 : 9 : 0. (A) Arrhenius plot. (B) Evolution of integrated OH area as a function of time on the Deacon stream during *T* variation. OH variation is expressed as the difference of the OH area at 1 : 9 : 0 feed and 703 K according to the fit at the corresponding time on stream and the actual measured area.

experiment is far from perfect. However, the major changes in acid/base character are satisfactorily deduced.

Although HRTEM is not statistically conclusive, there is nevertheless an indication that the well-faceted surface of CeO_2 becomes rounded during the course of the reaction. The evolution of the OH band intensity at $\sim$3730 cm^{-1} may be related to this morphological modification of the surface. Nevertheless, no activation corresponding to the increase in OH density was observed with our CeO_2 catalyst, and therefore a direct correspondence between the overall OH intensity and the reactivity should be excluded.

The oxygen pressure dependence of HCl oxidation over CeO_2 shows a positive $\sim$0.4–0.5 formal reaction order, even at high oxygen over-stoichiometry. Conversely, the effect of *p*HCl is positive (0.2–0.4) in high O_2 excess and gets negative for pHCl/pO_2 higher than $\sim$1.5.[8] This indicates that HCl activation is also an issue at low pHCl/pO_2, but O_2 activation is always difficult, essentially at all feed mixtures studied. Due to surface chlorination, low Cl coverage is likely not a factor for reactivity. Rather, if Cl coverage is high and/or Cl is too strongly bound, it blocks sites for elementary steps as HCl or O_2 activation.

The OH evolution in the pO_2 and *T* dependent *in situ* FTIR experiment indicated that higher pO_2 and *T* will increase the OH density, and concomitantly the reaction rate increased. This might be interpreted as lowering surface Cl concentration by opening up sites capable of abstracting H from HCl and shifting equilibrium coverage toward higher OH density. On the other hand, even in those feed conditions, under which increasing pO_2 would give rise to rate enhancement, *p*HCl was shown to increase reactivity with a concomitant decrease of OH density. These apparently opposite observations may be reconciled assuming the importance of repulsive lateral interactions (*e.g.* for HCl adsorption) in decreasing the heat of adsorption of surface species and thereby facilitating recombination and product desorption.

An alternative explanation may be related to surface restructuring as a function of pHCl/pO_2, which if facile could allow two parameters (structure and coverage) to control reactivity. Despite the rapid changes in the OH density following the variation in the parameter field studied, the above results and discussion suggest that one cannot assign the OH concentration *per se* as the main descriptor of HCl oxidation reactivity. Further studies correlating surface OH and Cl concentration may clarify details in HCl oxidation over ceria not accessible from this work (Table 1).

Conclusions

Ceria is widely used as support, catalyst, or co-catalyst for various catalytic processes. We utilised ceria as the main active phase for the heterogeneous catalytic HCl oxidation. Here we compared the acid/base properties of bulk ceria in its fresh and post-reaction states by probe molecule adsorption (CO_2, NH_3, CO) applying micro-calorimetry, FTIR, TPD and DFT calculations. The results indicate that the basic character of the ceria surface has been essentially eliminated upon reaction in HCl oxidation. This can be explained with the replacement of surface lattice O with Cl species and that the OH groups formed are rather acidic in nature. An *in situ* FTIR reaction cell has been developed in order to follow the evolution of OH groups during HCl oxidation. OH groups are reaction intermediates in HCl oxidation. The effect of experimental variables such as the reactant partial pressure and the reaction temperature was investigated. We find a good linear correlation of OH group density with the reactivity when T or pO_2 is varied. Nevertheless, an opposite trend is observed when pHCl is investigated, suggesting that the reactivity cannot be assigned to this sole surface parameter.

Acknowledgements

Bayer MaterialScience, the ICIQ Foundation, MICINN (CTQ2009-07753/BQU), BSC-RES are acknowledged for financial support. We thank Bayer MaterialScience for permission to publish these results.

Notes and references

1 T. Hibi, H. Abekawa, K. Seki, T. Suzuki, T. Suzuta, K. Iwanaga and T. Oizumi, EP936184, 1999.
2 T. Hibi, H. Nishida and H. Abekawa, *U.S. Patent* 5,871,707, 1999.
3 T. Hibi, T. Okuhara, K. Seki, H. Abekawa and H. Hamamatsu, WO200110550-A1, 2001.
4 A. Wolf, J. Kintrup, O. F. Schlüter and L. Mleczko, EP2027062, 2006.
5 A. Wolf, L. Mleczko, O. F. Schlüter and S. Schubert, EP2026905, 2006.
6 A. Wolf, L. Mleczko, S. Schubert and O. F. Schlüter, EP2027063, 2006.
7 J. Pérez-Ramírez, C. Mondelli, T. Schmidt, O. F. K. Schlüter, A. Wolf, L. Mleczko and T. Dreier, *Energy Environ. Sci.*, 2011, **4**, 4786–4799.
8 A. P. Amrute, C. Mondelli, M. Moser, G. Novell-Leruth, N. Lopez, D. Rosenthal, R. Farra, M. E. Schuster, D. Teschner, T. Schmidt and J. Pérez-Ramírez, *J. Catal.*, 2012, **286**, 287–297.
9 J. Ryczkowski, *Catal. Today*, 2001, **68**, 263–381.
10 A. Vimont, F. Thibault-Starzyk and M. Daturi, *Chem. Soc. Rev.*, 2010, **39**, 4928–4950.
11 F. C. Meunier, *Catal. Today*, 2010, **155**, 164–171.
12 G. Jacobs, L. Williams, U. Graham, G. A. Thomas, D. E. Sparks and B. H. Davis, *Appl. Catal., A*, 2003, **252**, 107–118.
13 R. Leppelt, B. Schumacher, V. Plzak, M. Kinne and R. J. Behm, *J. Catal.*, 2006, **244**, 137–152.
14 T. Shido and Y. Iwasawa, *J. Catal.*, 1993, **141**, 71–81.
15 X. Q. Wang, J. A. Rodriguez, J. C. Hanson, D. Gamarra, A. Martinez-Arias and M. Fernandez-Garcia, *J. Phys. Chem. B*, 2006, **110**, 428–434.
16 A. Goguet, F. C. Meunier, D. Tibiletti, J. P. Breen and R. Burch, *J. Phys. Chem. B*, 2004, **108**, 20240–20246.
17 D. Tibiletti, A. Goguet, D. Reid, F. C. Meunier and R. Burch, *Catal. Today*, 2006, **113**, 94–101.
18 J. D. Grunwaldt, M. Maciejewski, O. S. Becker, P. Fabrizioli and A. Baiker, *J. Catal.*, 1999, **186**, 458–469.
19 X.-S. Huang, H. Sun, L.-C. Wang, Y.-M. Liu, K.-N. Fan and Y. Cao, *Appl. Catal., B*, 2009, **90**, 224–232.
20 F. Romero-Sarria, L. M. Martinez, M. A. Centeno and J. A. Odriozola, *J. Phys. Chem. C*, 2007, **111**, 14469–14475.
21 O. Pozdnyakova, D. Teschner, A. Wootsch, J. Krohnert, B. Steinhauer, H. Sauer, L. Toth, F. C. Jentoft, A. Knop-Gericke, Z. Paal and R. Schlogl, *J. Catal.*, 2006, **237**, 1–16.
22 O. Pozdnyakova-Tellinger, D. Teschner, J. Kroehnert, F. C. Jentoft, A. Knop-Gericke, R. Schloegl and A. Wootsch, *J. Phys. Chem. C*, 2007, **111**, 5426–5431.
23 M. A. Hasan, M. I. Zaki and L. Pasupulety, *Appl. Catal., A*, 2003, **243**, 81–92.
24 Z. L. Wu, M. J. Li and S. H. Overbury, *J. Catal.*, 2012, **285**, 61–73.
25 G. Kresse and J. Hafner, *Phys. Rev. B: Condens. Matter Mater. Phys.*, 1993, **47**, 558–561.
26 J. P. Perdew, K. Burke and M. Ernzerhof, *Phys. Rev. Lett.*, 1996, **77**, 3865–3868.
27 M. Cococcioni and S. de Gironcoli, *Phys. Rev. B: Condens. Matter Mater. Phys.*, 2005, **71**, 035105.
28 S. Fabris, G. Vicario, G. Balducci, S. de Gironcoli and S. Baroni, *J. Phys. Chem. B*, 2005, **109**, 22860–22867.
29 M. V. Ganduglia-Pirovano, J. L. F. Da Silva and J. Sauer, *Phys. Rev. Lett.*, 2009, **102**, 026101.
30 P. E. Blöchl, *Phys. Rev. B: Condens. Matter Mater. Phys.*, 1994, **50**, 17953–17979.
31 H. J. Monkhorst and J. D. Pack, *Phys. Rev. B: Solid State*, 1976, **13**, 5188–5192.
32 H. Metiu, S. Chrétien, Z. Hu, B. Li and X. Sun, *J. Phys. Chem. C*, 2012, **116**, 10439–10450.
33 C. Li, Y. Sakata, T. Arai, K. Domen, K.-i. Maruya and T. Onishi, *J. Chem. Soc., Faraday Trans.*, 1989, **85**, 929–943.
34 G. N. Vayssilov, M. Mihaylov, P. S. Petkov, K. I. Hadjiivanov and K. M. Neyman, *J. Phys. Chem. C*, 2011, **115**, 23435–23454.

35 M. Nolan, S. C. Parker and G. W. Watson, *Phys. Chem. Chem. Phys.*, 2006, **8**, 216–218.
36 A. Badri, C. Binet and J.-C. Lavalley, *J. Phys. Chem.*, 1996, **100**, 8363–8368.
37 X. Gu, J. Ge, H. Zhang, A. Auroux and J. Shen, *Thermochim. Acta*, 2006, **451**, 84–93.
38 V. R. Choudhary and V. H. Rane, *J. Catal.*, 1991, **130**, 411–422.
39 K. I. Hadjiivanov and G. N. Vayssilov, *in Advances in Catalysis*, Academic Press, 2002, vol. 47, pp. 307–511.
40 O. V. Manoilova, S. G. Podkolzin, B. Tope, J. Lercher, E. E. Stangland, J.-M. Goupil and B. M. Weckhuysen, *J. Phys. Chem. B*, 2004, **108**, 15770–15781.
41 C. Binet, M. Daturi and J.-C. Lavalley, *Catal. Today*, 1999, **50**, 207–225.
42 G. A. H. Mekhemer and M. I. Zaki, *Adsorpt. Sci. Technol.*, 1997, **15**, 377–389.
43 M. Huang and S. Fabris, *J. Phys. Chem. C*, 2008, **112**, 8643–8648.
44 G. Busca, *Phys. Chem. Chem. Phys.*, 1999, **1**, 723–736.
45 G. Busca, in *Metal Oxide Catalysis*, ed. S. D. Jackson and J. S. J. Hargreaves, Wiley VCH, 2009, pp. 95–175.
46 J. A. Lercher, C. Gründling and G. Eder-Mirth, *Catal. Today*, 1996, **27**, 353–376.
47 K. Hauffe, H. Puschmann, K. Hauffe and H. Puschmann, *Corrosion Handbook*, Corrosion Handbook, Wiley VCH Frankfurt (Main), 2008.
48 A. Badri, C. Binet and J.-C. Lavalley, *J. Chem. Soc., Faraday Trans.*, 1996, **92**, 4669–4673.
49 D. Fernández-Torre, K. Kośmider, J. Carrasco, M. V. Ganduglia-Pirovano and R. Pérez, *J. Phys. Chem. C*, 2012, **116**, 13584–13593.